energies

MDPI

Article

State of Charge and State of Health Estimation of AGM VRLA Batteries by Employing a Dual Extended Kalman Filter and an ARX Model for Online Parameter Estimation

Ngoc-Tham Tran, Abdul Basit Khan and Woojin Choi *

Department of Electrical Engineering, Soongsil University, Seoul 06978, Korea; ngoctham87200@gmail.com (N.-T.T.); basit.kh@live.com (A.B.K.)
* Correspondence: cwj777@ssu.ac.kr; Tel.: +82-2-820-0652

Academic Editor: K.T. Chau
Received: 4 November 2016; Accepted: 14 January 2017; Published: 21 January 2017

Abstract: State of charge (SOC) and state of health (SOH) are key issues for the application of batteries, especially the absorbent glass mat valve regulated lead-acid (AGM VRLA) type batteries used in the idle stop start systems (ISSs) that are popularly integrated into conventional engine-based vehicles. This is due to the fact that SOC and SOH estimation accuracy is crucial for optimizing battery energy utilization, ensuring safety and extending battery life cycles. The dual extended Kalman filter (DEKF), which provides an elegant and powerful solution, is widely applied in SOC and SOH estimation based on a battery parameter model. However, the battery parameters are strongly dependent on operation conditions such as the SOC, current rate and temperature. In addition, battery parameters change significantly over the life cycle of a battery. As a result, many experimental pretests investigating the effects of the internal and external conditions of a battery on its parameters are required, since the accuracy of state estimation depends on the quality of the information regarding battery parameter changes. In this paper, a novel method for SOC and SOH estimation that combines a DEKF algorithm, which considers hysteresis and diffusion effects, and an auto regressive exogenous (ARX) model for online parameters estimation is proposed. The DEKF provides precise information concerning the battery open circuit voltage (OCV) to the ARX model. Meanwhile, the ARX model continues monitoring parameter variations and supplies information on them to the DEKF. In this way, the estimation accuracy can be maintained despite the changing parameters of a battery. Moreover, online parameter estimation from the ARX model can save the time and effort used for parameter pretests. The validation of the proposed algorithm is given by simulation and experimental results.

Keywords: state of charge; state of health; auto regressive exogenous (ARX) model; dual extended Kalman filter (DEKF); idle stop-start systems

1. Introduction

The growing awareness of global warming, fossil fuel depletion and fuel cost escalation have resulted in opportunities for the development of the automotive industry in terms of increasing vehicle efficiency and reducing carbon dioxide (CO_2) emissions. As a result, a lot of effort has been made to improve the efficiency of conventional engine based vehicles. In order to satisfy the need for improved fuel efficiency, idle stop start systems (ISS) systems are favored as a key operation strategy since they can improve fuel efficiency and reduce emissions by eliminating the fuel consumption that would normally be spent to keep the engine running when a vehicle is not moving. For this type of system, frequent system starts and stops are required. As a result, the batteries undergo a lot of stress from experiencing very different heavy load characteristics. Since the failure to restart an engine would be

a serious problem in the operation of a vehicle, the state of charge (SOC) and state of health (SOH) of batteries is a critical concern. This is also particularly important for the efficient utilization of a battery and to optimize the performance, extend the lifetime, and prevent progressive irreversible damage to batteries. Typically a lead-acid battery is used for these applications. In particular, the absorbent glass mat valve regulated lead-acid (AGM VRLA) type battery is favored because it can handle the deep cycling requirements of highly frequent starts. It is also able to receive a dynamic charge, which makes it more effective for regenerative braking and allows for a more aggressive idle start stop strategy. In addition, AGM VRLA batteries demonstrate a long service lifetime and are completely maintenance-free [1].

Since lead-acid batteries have nonlinear characteristics such as the hysteresis effect, their SOC and SOH estimation is more challenging than for other kinds of batteries [2,3]. In [4], the relationship between the discharge voltage and the SOC was determined for a wide range of discharge rates at different ambient temperatures for telecommunication backup power supply applications. However, since this relationship is not applicable to random discharge currents, this method has a large SOC error (up to 10%). In [5], an SOC estimation technique for lead-acid batteries using a combination of the terminal voltage, the battery impedance and the charge current of the battery was proposed. A novel equivalent circuit model of a lead-acid battery taking into account the diffusion and the sulphation effects was proposed, and the parameter estimation was successfully performed using recursive least squares (RLS) method. However, the method was only developed to estimate the SOC. The method presented in [6] adopted a two-current-pulse test to determine the model parameters of the battery. Then the parameters were used to find the SOC and SOH of a VRLA battery. However, this method is an off-line method that requires a large number of tests to determine the battery model parameters at different SOCs and SOHs of a VRLA battery. As a result, this method is not practical to use. In [7], the SOC and SOH of a VRLA battery was estimated using a dual extended Kalman filter (DEKF). However, its estimation accuracy cannot be maintained if the operating temperature varies or if the battery becomes aged since the parameters of the battery model are not estimated online. A method to utilize an extended Kalman filter (EKF) and fuzzy logic for SOC and SOH estimation was proposed in [8]. However, the SOH of the battery can only be accurately determined when the battery is continuously charged or discharged. As a result, this method is not suitable for practical applications.

Online parameter estimation for the equivalent circuit model of a battery has been introduced in several previous studies. In [9], a data driven method using the RLS technique was proposed to determine the lumped parameters of a battery model. It combined a data driven method and an adaptive EKF for the SOC estimation of lithium-ion polymer batteries. In [10], an auto regressive exogenous (ARX) model to determine the model parameters of a $LiFePO_4$ battery and an order selection for the ARX model were proposed and discussed. Reference [11] introduced an invariant imbedding method (IIM) to estimate the model parameters of a $LiFePO_4$ battery. A similar approach has been introduced in [12], where several RC networks are used to model the polarization characteristics of a lithium-ion battery using the RLS method to estimate the parameters. In all of the above mentioned methods for parameter estimation [9–12], lithium-ion batteries were used and the parameter estimation was verified for a very short period of time. In most of these cases, monotonously decreasing SOC (from 100% SOC to 0% SOC) profiles were used to verify the performances of the proposed methods. Since parameters vary at different ageing levels and different operating temperatures, algorithms must be verified under those conditions. Due to the fact that lithium-ion batteries do not have a significant hysteresis effect, their SOC estimation is a lot easier when compared to that of AGM VRLA batteries.

In order to estimate SOC and SOH, several methods have been applied including Coulomb counting, fuzzy logic (FL), artificial neural networks (ANNs), EKF and etc. [13–31]. The Coulomb counting or current integration method, which measures the amount of charge taken out of or put into a battery in terms of ampere hours, is simple and has a low computational burden. However, in order to achieve SOC estimation with this method, the initial SOC must be known. Furthermore, accumulated measurement errors might be the source of a significant inaccuracy for the SOC estimation. As a

result, an additional recalibration may be required when the ampere hours counting is performed over a long period of time. The ANNs and FL approaches can estimate the SOC of a battery with an arbitrary initial SOC value [22–26]. The robustness of these models relies a lot on the quantity and the quality of the training data set. A limited training data set may result in a limited model robustness, which reduces the applicability of these methods. The EKF approach is a computationally efficient recursive digital processing technique used to estimate the state of a nonlinear dynamic system from a series of incomplete and noisy measurements in a way that minimizes the mean squared error [14,27,28]. A DEKF including two adaptive filters is used to estimate both the SOC and the battery capacity [27]. The DEKF is an intelligent and optimal method for estimating the state of a dynamic system. In addition, it automatically provides the dynamic error bounds of the estimation. Consequently, the DEKF approach is preferred among the above mentioned methods due to its advantages and ability to provide reliable results. However, the DEKF can only give reliable results under the assumption that the model is accurate. Unfortunately, battery parameter characteristics change over the battery lifetime. As a result, the estimation accuracy deteriorates as time goes by. Furthermore, the battery parameters are highly dependent on the battery operation conditions such as the SOC, temperature and current rate [29–31]. Thus, a lot of pretests are required to obtain information concerning parameter changes. This information is then provided to the DEKF to achieve accurate estimations. However, this is a time consuming process that is error prone and requires a lot of instruments and human labor. Therefore, online parameters estimation can provide a lot of benefits in terms of reducing the time and labor for pretests and in increasing the accuracy of SOC and SOH estimation even when the parameters of a battery change.

In this study, a novel method which combines the DEKF and ARX methods while considering hysteresis and diffusion effects is proposed for the SOC and SOH estimation of AGM VRLA batteries. The major contributions of this paper can be summarized as follows:

1. The nonlinear characteristics of lead-acid batteries such as the hysteresis and diffusion effects have been modeled accurately and the error in the SOC estimation is less than 5%.
2. Unlike the conventional approaches, the SOC and SOH estimation performance has been tested with batteries with different aging levels under the varying temperature conditions and reliable results have been obtained under extensive variations in temperature, SOC and current.
3. The reliability of the proposed method in terms of estimating the SOC and SOH have been verified through very long test profiles (about 100 h for the SOC estimation and 440 h for the SOH estimation) with both the charging and discharging cycles.
4. To test the performance in estimating the SOH, three different initial values have been given to verify its convergence characteristics by using a 440 h test profile.

2. Battery Model

The battery electric equivalent circuit consists of an open circuit voltage (OCV) connected in series with an internal resistance R_i and R-C parallel branch of the charge transfer resistance R_{tc} along with a double layer capacitance C_{dl} to obtain the voltage response from the battery current [2,3]. This battery model is simple and effective. As a result, it can be easily applied in practical applications. The reconstruction voltage response of the battery includes two parts: the OCV and the dynamic effect voltage drop on the battery parameters as shown in Figure 1.

The SOC-OCV model including the hysteresis and diffusion effects can be shown as:

$$\begin{aligned} \mathrm{OCV}(\mathrm{SOC},\alpha,\zeta) \;=\; & \alpha\,[(1-\zeta)\mathrm{OCV}_{\mathrm{c3h}}(\mathrm{SOC})+\zeta\mathrm{OCV}_{\mathrm{c3m}}(\mathrm{SOC})] \\ & +(1-\alpha)\,[(1-\zeta)\mathrm{OCV}_{\mathrm{d3h}}(\mathrm{SOC})+\zeta\mathrm{OCV}_{\mathrm{d3m}}(\mathrm{SOC})] \end{aligned} \tag{1}$$

where ζ is the diffusion factor calculated by a first order exponential function with respect to the relaxation time. The hysteresis factor α is determined by a normalized integration of the charge throughput. $\mathrm{OCV}_{\mathrm{c3h}}(\mathrm{SOC})$, $\mathrm{OCV}_{\mathrm{c3m}}(\mathrm{SOC})$, $\mathrm{OCV}_{\mathrm{d3h}}(\mathrm{SOC})$, and $\mathrm{OCV}_{\mathrm{d3m}}(\mathrm{SOC})$, are the charge OCV

with 3 h relaxation, the charge OCV with 3 min relaxation, the discharge OCV with 3 h relaxation, and the discharge OCV with 3 min relaxation, respectively. The factors and equations mentioned above were demonstrated in previous studies [2,3].

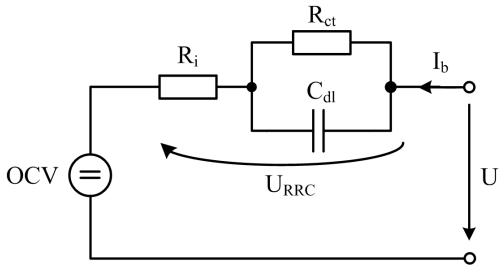

Figure 1. Selected model for the lead-acid battery.

3. Battery Parameters Estimation

3.1. ARX Model

Some methods such as Box-Jenkins (BJ), auto regressive moving average exogenous (ARMAX), auto regressive moving average (ARMA) and ARX can be used for battery parameter estimation [32]. The Box-Jenkins model in Equation (2), which contains both an input and model error, is the most general parametric linear system model. However, the disadvantage of this model is its heavy computational burden:

$$y(t) = \frac{B(q)}{F(q)}\, u(t) + \frac{C(q)}{D(q)}\, e(t) \tag{2}$$

The ARMA model in Equation (3) can be seen as a Box-Jenkins (or ARMAX) structure without consideration of the input component:

$$y(t) = \frac{B(q)}{A(q)}\, e(t) \tag{3}$$

The ARMAX model in Equation (4), which has become a standard tool both for system identification and control design, is similar to a Box-Jenkins model [32]. It can be achieved by changing the denominator of the output and the process noise, $A(q) = D(q)$:

$$y(t) = \frac{B(q)}{A(q)}u(t) + \frac{C(q)}{A(q)}e(t) \tag{4}$$

The ARX structure in Equation (5) is considered to be a specific case of the ARMAX model by setting the numerator of the process noise to 1, $C(q) = 1$:

$$y(t) = \frac{B(q)}{A(q)}u(t) + \frac{1}{A(q)}e(t) \tag{5}$$

where y is the output sequence and u is the input sequence. In addition, $A(q)$, $B(q)$, $C(q)$, $D(q)$ and $F(q)$ are polynomials with respect to the forward shift operator q and are defined by the following equations:

$$A(q) = 1 + a_1 q^{-1} + \ldots + a_{n_a} q^{-n_a} \tag{6}$$

$$B(q) = b_0 + b_1 q^{-1} + \ldots + b_{n_b} q^{-n_b} \tag{7}$$

$$C(q) = 1 + c_1 q^{-1} + \ldots + c_{n_c} q^{-n_c} \tag{8}$$

$$D(q) = 1 + d_1 q^{-1} + \ldots + d_{n_d} q^{-n_d} \tag{9}$$

$$F(q) = 1 + f_1 q^{-1} + ... + f_{n_f} q^{-n_f} \tag{10}$$

Since it is the simplest model that can involve the input and additive noise, the ARX model is applied in this paper for the battery parameter estimation. An n^{th} order linear time variant ARX model is given by:

$$y(k) + a_1 y(k-1) + ... + a_n y(k-n) = b_0 u(k) + b_1 u(k-1) + ... + b_m u(k-m) + e(k) \tag{11}$$

There is a practical way for Equation (11) to determine the next output value given by the previous observation and the prediction error as shown in Equation (12):

$$y(k) = -a_1 y(k-1) - ... - a_n y(k-n) + b_0 u(k) + b_1 u(k-1) + ... + b_m u(k-m) + e(k) \tag{12}$$

To achieve a more compact notation, Equation (12) can be rewritten as:

$$y(k) = \varphi^T(k)\theta(k-1) + e(k) \tag{13}$$

where:

$$\theta = [a_1, ..a_n, b_0, b_1, ..., b_m]^T \tag{14}$$

$$\varphi(k) = [-y(k-1), ..., -y(k-n), u(k), u(k-1), u(k-m)]^T \tag{15}$$

The additive noise term $e(k)$ is entered as direct noise in the difference Equation (11). The parameters n and m are model orders where the order of the auto-regression term n and the moving average term m aim to simulate the cell nonlinear dynamics. The model structures, such as Equation (13), that are linear in θ are known in statistics as linear regressions. The vector $\varphi(k)$ is called a regression vector, and its components are regressors [32].

The electrical behavior of the equivalent circuit model of a battery can be expressed by Equation (16) in the frequency domain:

$$U(s) = OCV(s) + I_b(s)R_i + I_b(s)\frac{R_{ct}}{(R_{ct}C_{dl})s + 1} \tag{16}$$

where $U(s)$ is the battery terminal voltage, $I_b(s)$ is the battery current with a negative value in the discharge state and a positive value in the charge state, and s is the frequency operator. The voltage U_{RRC}, which drops on the R_i and R_{ct}–C_{dl} network, can be expressed in Equation (17) as follows:

$$U_{RRC}(s) = U(s) - OCV(s) = I_b(s)R_i + I_b(s)\frac{R_{ct}}{(R_{ct}C_{dl})s + 1} \tag{17}$$

The transfer function $G(s)$ of Equation (16) can be written as Equation (18):

$$G(s) = \frac{U_{RRC}(s)}{I_b(s)} = R_i + \frac{R_{ct}}{(R_{ct}C_{dl})s + 1} = \frac{(R_i R_{ct} C_{dl})s + R_i + R_{ct}}{(R_{ct}C_{dl})s + 1} \tag{18}$$

Using the bilinear transformation method shown in Equation (19) as a transfer function $G(s)$, the discrete transfer function of a battery system with a sample time of T can be performed in Equation (20):

$$s = \frac{2}{T}\frac{1 - z^{-1}}{1 + z^{-1}} \tag{19}$$

where z is the discretization operation:

$$G(z^{-1}) = \frac{\frac{R_i T + R_{ct} T + 2R_i R_{ct} C_{dl}}{T + 2R_{ct} C_{dl}} + \frac{R_i T + R_{ct} T - 2R_i R_{ct} C_{dl}}{T + 2R_{ct} C_{dl}} z^{-1}}{1 + \frac{T - 2R_{ct} C_{dl}}{T + 2R_{ct} C_{dl}} z^{-1}} = \frac{b_0 + b_1 z^{-1}}{1 + a_1 z^{-1}} \tag{20}$$

where:

$$a_1 = \frac{(T - 2R_{ct}C_{dl})}{(T + 2R_{ct}C_{dl})}$$

$$b_0 = \frac{(R_iT + R_{ct}T + 2R_iR_{ct}C_{dl})}{(T + 2R_{ct}C_{dl})}$$

$$b_1 = \frac{(R_iT + R_{ct}T - 2R_iR_{ct}C_{dl})}{(T + 2R_{ct}C_{dl})}$$

The time domain relationship between different samples of input/output is as follows:

$$U(k) - OCV(k) = -a_1(U(k-1) - OCV(k-1)) + b_0I_b(k) + b_1I_b(k-1) \quad (21)$$

The above function is a specific form of the ARX model in Equation (12) for the equivalent circuit model with first order:

$$y(k) = -a_1y(k-1) + b_0u(k) + b_1u(k-1) \quad (22)$$

3.2. Parameters Estimation Algorithm

By applying a RLS algorithm that can track the time variant parameters of the dynamic process model to estimate the coefficient factors, the system identification can be realized by the following steps [32]. The prediction error of the voltage U_{RRC}:

$$e(k) = U_{RRC}(k) - \varphi^T(k)\hat{\theta}(k-1) \quad (23)$$

The updated gain of the RLS algorithm:

$$L(k) = \frac{P(k-1)\varphi(k)}{\lambda(k) + \varphi^T(k)P(k-1)\varphi(k)} \quad (24)$$

The estimated coefficient vector:

$$\hat{\theta}(k) = \hat{\theta}(k-1) + L(k)[U_{RRC}(k) - \varphi^T(k)\hat{\theta}(k-1)] \quad (25)$$

The covariance matrix of the estimated coefficient vector:

$$P(k) = \frac{1}{\lambda(k)}\left[P(k-1) - \frac{P(k-1)\varphi(k)\varphi^T(k)P(k-1)}{\lambda(k) + \varphi^T(k)P(k-1)\varphi(k)}\right] \quad (26)$$

Specifically:

$$\varphi(k) = [-U_{RRC}(k-1), I_b(k), I_b(k-1)]^T \quad (27)$$

$$\theta(k) = [a_1(k), b_0(k), b_1(k)]^T \quad (28)$$

where $\varphi(k)$ is the input vector obtained from input data values including the dynamic effect voltage $U_{RRC}(k-1)$ drop on the battery parameters at the time index $k-1$, and the battery currents $I(k)$ and $I(k-1)$ at the time steps k and $k-1$, respectively. $\theta(k)$ is the coefficient vector, which needs to be identified. $\lambda(k)$ $(0 < \lambda < 1)$ is the forgetting factor which can be used to give greater weight to recent data than older data.

The estimated coefficient vector $\hat{\theta}(k)$ at the time index k in Equation (28) is updated by adding a correction to the coefficient vector at the time index $k-1$, which is the difference between the battery terminal measured voltage $y(k)$ and the estimated voltage and the update gain $L(k)$. The error of the

coefficient vector is reduced recursively. After identifying $a_1(k)$, $b_0(k)$, and $b_1(k)$, the parameters of the battery model at each time step can be determined as:

$$R_i(k) = \frac{b_1(k) - b_0(k)}{a_1(k) - 1} \tag{29}$$

$$R_{ct}(k) = \frac{2a_1(k)b_0(k) - 2b_1(k)}{(a_1(k) - 1)(a_1(k) + 1)} \tag{30}$$

$$C_{dl}(k) = \frac{T(a_1(k) - 1)^2}{4(b_1(k) - a_1(k)b_0(k))} \tag{31}$$

4. Combination of a Dual Extended Kalman Filter and an ARX Model for SOC and SOH Estimation

The battery parameters estimated by the ARX method in Section 3 are then used for estimating the SOC using the DEKF algorithm. The combination of the two methods is depicted in Figure 2. The DEKF obtains exact information on the OCV of the battery and gives it to the ARX model. Meanwhile, the ARX model continues observing the parameter variations by the RLS with the forgetting factor and gives them to the DEKF. By following this procedure, the estimation accuracy can be maintained even if the parameters of the battery change.

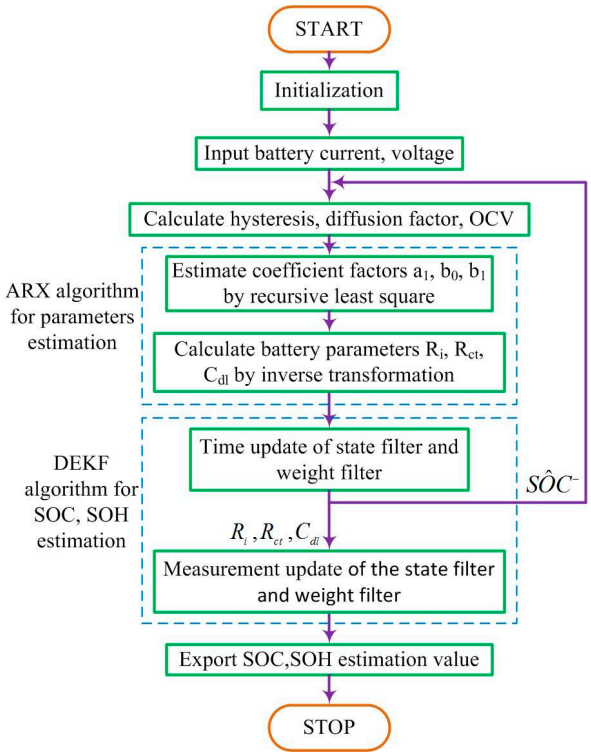

Figure 2. The proposed flowchart of the combination of ARX model and DEKF algorithm.

The DEKF framework, which is described in Equations (32) to (50), contains the two EKFs. One of them is a state filter used for estimating the SOC, and the other is a weight filter which estimates the battery capacity [15]. In each time step, the state filter uses the priori value of the weight filter, and vice versa. Thus, the two adaptive filters interact with each other and simultaneously estimate the SOC and capacity. Nonlinear state space models of the DEKF algorithm including the process, the measurement model of the state filter and the capacity of the weight filter are derived in Equations (34)–(36), respectively. The process model defines the SOC and the voltage V_{Cdl} drops

on the R_{ct}-C_{dl} circuit, while the measurement model expresses the battery estimated voltage y based on the battery model in Figure 1. By determining the SOC and battery capacity as members of the state model, the DEKF algorithm automatically estimates accurate values of SOC and SOH. Nonlinear state-space models can be represented by Equations (32) and (33):

$$\mathrm{x}_{k+1} = \mathrm{f}(\mathrm{x}_k, \mathrm{u}_k, \theta_k) + \mathrm{w}_k,\ \theta_{k+1} = \theta_k + \mathrm{r}_k \tag{32}$$

$$\mathrm{y}_k = \mathrm{g}(\mathrm{x}_k, \mathrm{u}_k, \theta_k) + \mathrm{v}_k,\ \mathrm{d}_k = \mathrm{g}(\mathrm{x}_k, \mathrm{u}_k, \theta_k) + \mathrm{e}_k \tag{33}$$

where x_k is the state vector of the battery model, θ_k is the time varying battery capacity, u_k is the exogenous input, V_k is the system output, and w_k, v_k, r_k and e_k are independent Gaussian noise processes with the covariance matrices ${Q_k}^x$, ${R_k}^x$, ${Q_k}^\theta$ and ${R_k}^\theta$, respectively. $f(.,.,.)$ represents a nonlinear transition matrix function and $g(.,.,.)$ represents a nonlinear measurement matrix.

The state space equation for the proposed battery model in Figure 1 can be represented in discrete form as Equations (34) and (35):

$$\mathrm{x}_{k+1} = \begin{pmatrix} z_{k+1} \\ V_{Cdl,k+1} \end{pmatrix} = \begin{pmatrix} 1 & 0 \\ 0 & 1 - \frac{\Delta t}{R_{tc}C_{dl}} \end{pmatrix} \begin{pmatrix} z_k \\ V_{Cdl,k} \end{pmatrix} + \begin{pmatrix} \frac{\eta_i \Delta t}{C_b} & \frac{\Delta t}{C_{dl}} \end{pmatrix}^T I_{b,k} + w_k \tag{34}$$

$$\theta_k = [C_{b,k}] \tag{35}$$

The terminal voltage of the battery model can be represented using a nonlinear function as follows:

$$U_k = \mathrm{OCV}(z_k, \zeta_k, \alpha_k) + V_{Cdl,k} + R_i I_k + v_k \tag{36}$$

The computing procedure for the DEKF can be summarized as follows [15]:

Step 1: Initialization at k = 0:

$$\begin{aligned} \hat{\theta}_0^+ &= \mathrm{E}[\mathrm{x}_0],\ \hat{\mathrm{P}}_{\tilde{\theta},0}^+ = \mathrm{E}\left[\left(\theta_0 - \hat{\theta}_0^+\right)\left(\theta_0 - \hat{\theta}_0^+\right)^T\right] \\ \hat{x}_0^+ &= \mathrm{E}[\mathrm{x}_0],\ \hat{\mathrm{P}}_{\tilde{x},0}^+ = \mathrm{E}\left[\left(\mathrm{x}_0 - \hat{x}_0^+\right)\left(\mathrm{x}_0 - \hat{x}_0^+\right)^T\right] \end{aligned} \tag{37}$$

where, E[.] is the statistical expectation operator.

Step 2: Approximation of nonlinear functions:

$$\mathrm{F}_{k-1} = \left.\frac{\partial \mathrm{f}(\mathrm{x}_{k-1}, \mathrm{u}_{k-1}, \hat{\theta}_k^-)}{\partial \mathrm{x}_{k-1}}\right|_{x_{k-1}=\hat{x}_{k-1}^+} = \begin{pmatrix} 1 & 0 \\ 0 & 1 - \frac{\Delta t}{R_{tc}C_{dl}} \end{pmatrix} \tag{38}$$

$$\mathrm{G}_k^x = \left.\frac{\partial \mathrm{g}\left(\mathrm{x}_k, \mathrm{u}_k, \hat{\theta}_k^-\right)}{\partial \mathrm{x}_k}\right|_{x_k=\hat{x}_k^-} = \begin{bmatrix} \sum_{i=0}^{4} (i+1) a_{i,k} \left(z_k^-\right)^i & -1 \end{bmatrix} \tag{39}$$

$$\mathrm{G}_k^\theta = \left.\frac{d\mathrm{g}\left(\mathrm{x}_k, \mathrm{u}_k, \hat{\theta}_k^-\right)}{d\theta}\right|_{\theta=\hat{\theta}_k^-} = \frac{\partial g\left(\widehat{x}_k^-, u_k, \theta\right)}{\partial \theta} + \frac{\partial g\left(\widehat{x}_k^-, u_k, \theta\right)}{\partial \widehat{x}_k^-} \frac{d\widehat{x}_k^-}{d\theta} \tag{40}$$

where:

$$\frac{d\widehat{x}_k^-}{d\theta} = \frac{\partial f\left(\widehat{x}_{k-1}^+, u_{k-1}, \theta\right)}{\partial \theta} + \frac{\partial f\left(\widehat{x}_{k-1}^+, u_{k-1}, \theta\right)}{\partial \widehat{x}_k^+} \frac{d\widehat{x}_{k-1}^+}{d\theta}$$

$$\frac{d\widehat{x}_{k-1}^+}{d\theta} = \frac{d\widehat{x}_{k-1}^-}{d\theta} - L_{k-1}^x \frac{dg\left(\widehat{x}_{k-1}^-, u_{k-1}, \theta\right)}{d\theta}$$

The partial derivatives are computed at each time step, while the total derivatives are computed recursively with zeros as their initial values.

Step 3: Time update of each filter.

State filter:

$$\hat{x}_k^- = \mathrm{f}(\hat{x}_{k-1}^+, \mathrm{u}_{k-1}, \hat{\theta}_k^-) \tag{41}$$

$$\mathrm{P}_{x,k}^- = \mathrm{F}_{k-1}\mathrm{P}_{x,k-1}^+\mathrm{F}_{k-1}^T + \mathrm{Q}_k^x \tag{42}$$

Weight filter:

$$\hat{\theta}_k^- = \hat{\theta}_{k-1}^+ \tag{43}$$

$$\mathrm{P}_{\theta,k}^- = \mathrm{P}_{\theta,k-1}^+ + \mathrm{Q}_k^\theta \tag{44}$$

Step 4: Measurement update of each filter.

State filter:

$$\mathrm{K}_k^x = \mathrm{P}_{x,k}^-(\mathrm{G}_k^x)^T\left[\mathrm{G}_k^x\mathrm{P}_k^-(\mathrm{G}_k^x)^T + \mathrm{R}_k^x\right]^{-1} \tag{45}$$

$$\hat{x}_k^+ = \hat{x}_k^- + \mathrm{K}_k^x\left[\mathrm{y}_k - \mathrm{g}\left(\hat{x}_k^-, \mathrm{u}_k, \hat{\theta}_k^-\right)\right] \tag{46}$$

$$\mathrm{P}_{x,k}^+ = (\mathrm{I} - \mathrm{K}_k^x\mathrm{G}_k^x)\mathrm{P}_{x,k}^- \tag{47}$$

Weight filter:

$$\mathrm{K}_k^\theta = \mathrm{P}_{\theta,k}^-\left(\mathrm{G}_k^\theta\right)^T\left[\mathrm{G}_k^\theta\mathrm{P}_k^-\left(\mathrm{G}_k^\theta\right)^T + \mathrm{R}_k^\theta\right]^{-1} \tag{48}$$

$$\hat{\theta}_k^+ = \hat{\theta}_k^- + \mathrm{K}_k^\theta\left[\mathrm{y}_k - \mathrm{g}\left(\hat{x}_k^-, \mathrm{u}_k, \hat{\theta}_k^-\right)\right] \tag{49}$$

$$\mathrm{P}_{\theta,k}^+ = \left(\mathrm{I} - \mathrm{K}_k^\theta\mathrm{G}_k^\theta\right)\mathrm{P}_{\theta,k}^- \tag{50}$$

5. Experimental Validation

In order to validate the proposed algorithm, a dynamic charge discharge current profile is applied to the battery for the SOC estimation validation process. This profile contains frequent charge discharge currents and operates in high and mid SOC ranges, which is a typical battery use case in automotive applications. The battery used for the test is a 12 V, 70 Ah AGM70L—DIN battery (Solite, Belmore, New South Wales, Australia) and it is connected to a bipolar DC power supply NF BP4610. A program created in Labview version 11.0 automatically controls the output of the bipolar DC power supply. It also records the voltage and current of the battery through a NI myDAQ device from National Instruments (Austin, TX, USA) and a sensing circuit. The battery current and voltage are measured at constant time intervals for 1s during the test. The SOC reference profile is calculated using the Coulomb counting method on the measured current data. First, the battery is fully charged by the CC-CV (constant current and constant voltage) method to obtain the correct initial value of the SOC. Then the battery is allowed to rest for 3 h to return it to an electrochemical and thermal equilibrium condition before applying the test profile. Moreover, to guarantee the operation of the proposed method for estimating the battery capacity, a pulse current test comprised of a sequence of discharge pulses and relaxation followed by a sequence of charge pulses and relaxation was conducted. The terminal voltage and current of the battery were recorded by a host computer and data acquisition board every second during the 440 h test. Then, the combined method of an online parameter estimation algorithm by the ARX model and a SOC and SOH estimation by the DEKF is implemented in the Labview environment, and the voltage and current sequences obtained during the dynamic charge discharge test are used as input data. Three batteries of the same type (Nominal Capacity (Cn) = 70 Ah), but having different measured capacities (98%, 75.6% and 59.3%) due to ageing, are used to validate the SOC and SOH estimation algorithm.

First, the estimation results obtained with the proposed algorithm for the battery having 98% of its nominal capacity (68.6 Ah) are shown in Figures 3–5. The middle graph of Figure 3 shows a comparison of the measured and simulated battery voltages obtained with the proposed DEKF-ARX method, and the simulated voltage obtained with the conventional DEKF method. Meanwhile, the relative error between the voltages is shown in the lower graph as a function of time. As illustrated in the lower graph of Figures 3 and 4, the voltage estimations obtained from the simulation shows that the DEKF-ARX method provides better results in terms of voltage estimation. The maximum voltage estimation error is about 0.1 V for the DEKF-ARX method, while it is more than 0.1 V in case of the conventional DEKF method.

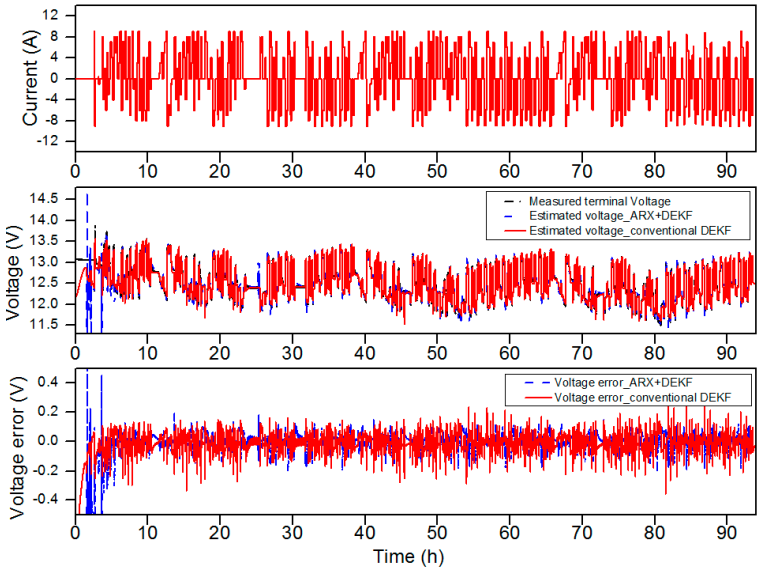

Figure 3. Current profile (**upper** graph), measurement voltage and estimated voltage comparison (**middle** graph) and voltage estimation error (**lower** graph).

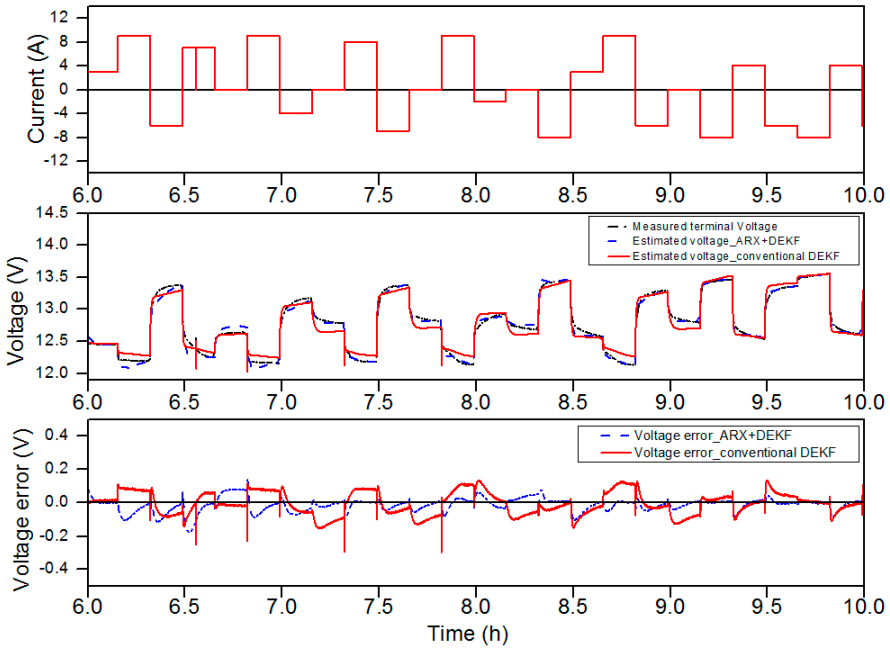

Figure 4. Zoomed in version of Figure 3.

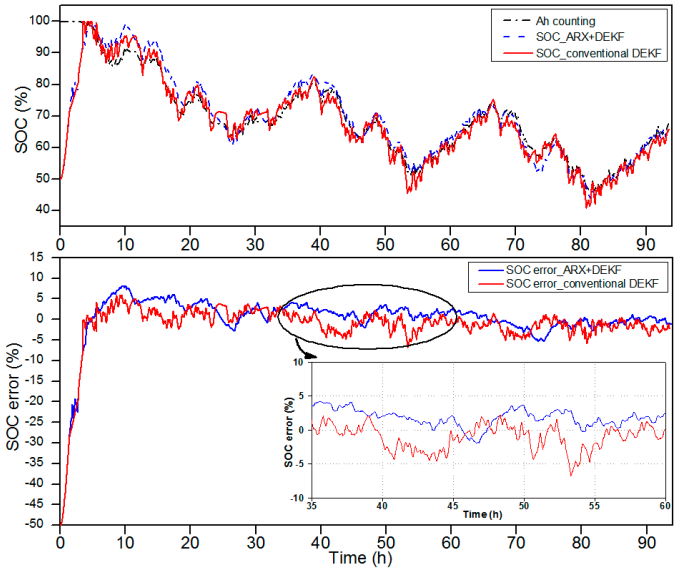

Figure 5. Comparison of the SOC estimation for the first battery (98% SOH) by the proposed ARX-DEKF and conventional DEKF method.

The upper graph of Figure 5 depicts a comparison between the simulated SOC by the DEKF-ARX method, the simulated SOC by the conventional DEKF method and the Coulomb counting reference profile, while the SOC estimation error in percentages for both methods are shown in the lower graph of Figure 4. The initialization of the estimated SOC was 50% instead of 100% to verify that the proposed algorithm converges to the true SOC value. After 10 h of operation, the SOC error is reduced to 8% and it remains less than 5% for the DEKF-ARX method. Meanwhile the SOC estimation error of the conventional DEKF method increases to 7%.

The capacity estimation of a fresh battery with a 98% capacity is shown in Figure 6. The three different initial capacity values used in the simulation are 0.8 Cn, 1.2 Cn and 1.0 Cn. In all three cases, the estimated values of the capacity converge to the right capacity (0.98 Cn = 68.6 Ah) within an error range of 3%.

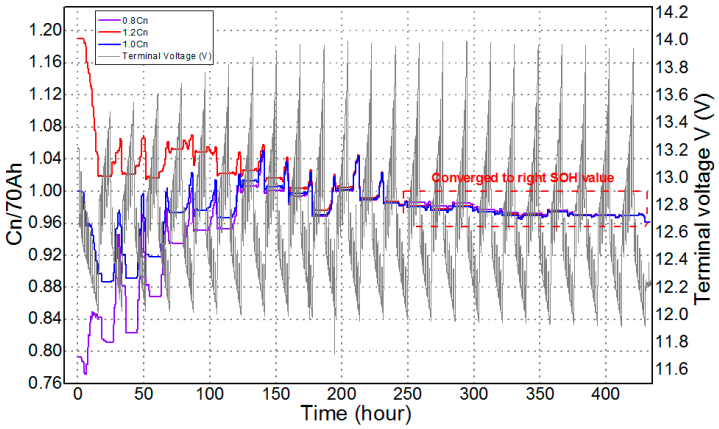

Figure 6. The convergence of the SOH estimation result with different initial capacity values (The measured capacity of the battery is 98% SOH).

The estimation results obtained with the proposed algorithm for a battery with a 75.6% measured capacity are shown in Figures 7–9. These results also demonstrate the improved estimation provided by the DEKF-ARX method.

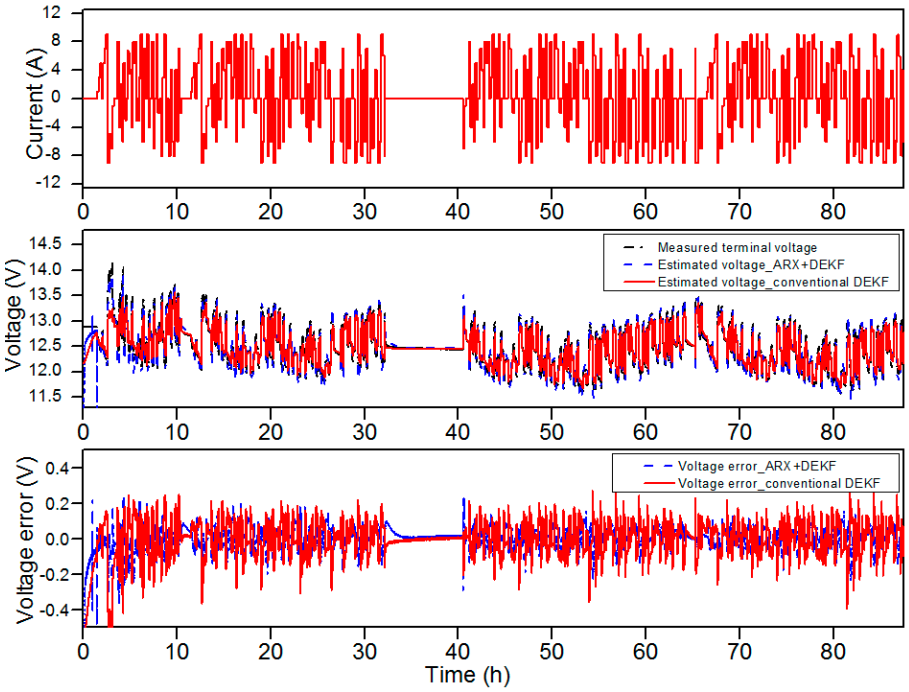

Figure 7. Comparison of the terminal voltage estimation for the aged battery (75.6% SOH) by the proposed ARX DEKF and conventional DEKF method.

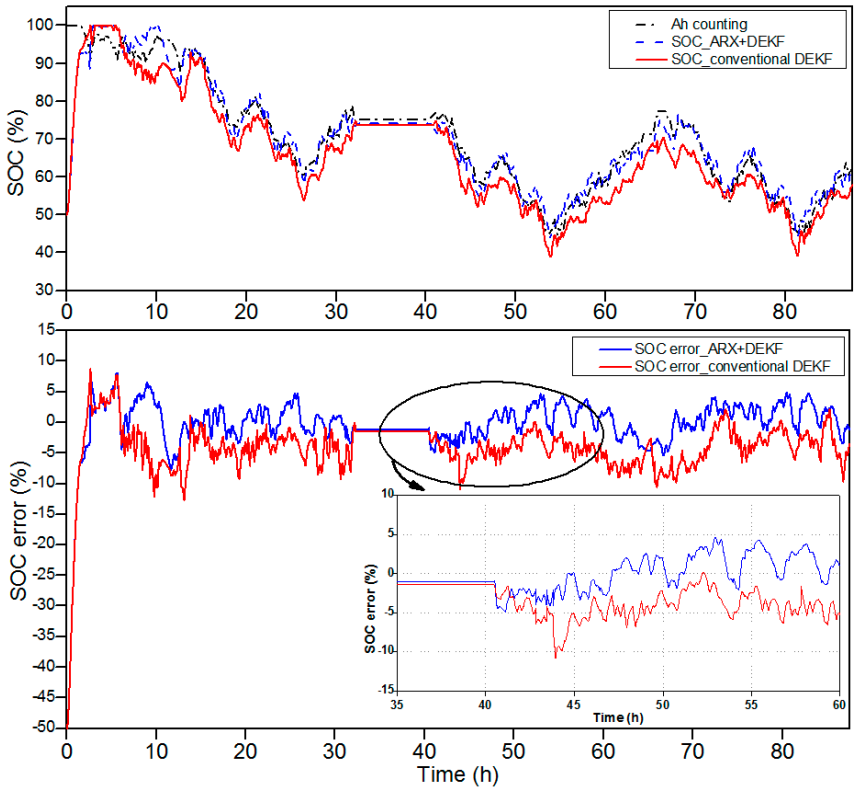

Figure 8. Comparison of the SOC estimation for the aged battery (75.6% SOH) by the proposed ARX-DEKF and conventional DEKF method.

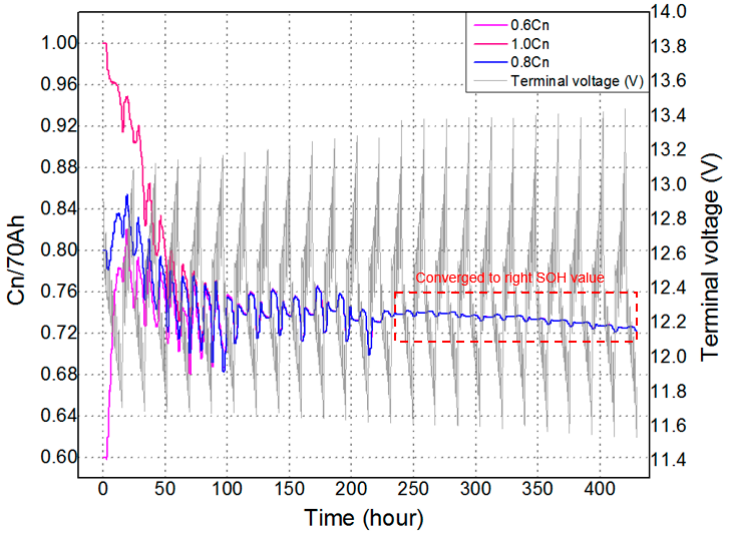

Figure 9. The convergence of the SOH estimation result with different initial capacity values (The measured capacity of the battery is 75.6% SOH).

Figure 9 shows the capacity estimation of an aged battery with a 75.6% measured capacity with the DEKF-ARX method. The three different initial capacity values used in the simulation are 1.0 Cn, 0.8 Cn and 0.6 Cn. In all three cases, the estimated values of the capacity converge to the real capacity (0.756 Cn = 52.92 Ah) within an error range of 3%.

Similarly, the estimation results obtained with the proposed method for a battery with a 59.3% measured capacity are shown in Figures 10–12. Figure 11 clearly shows the supremacy of the DEKF-ARX method over the conventional DEKF method in term of SOC estimation.

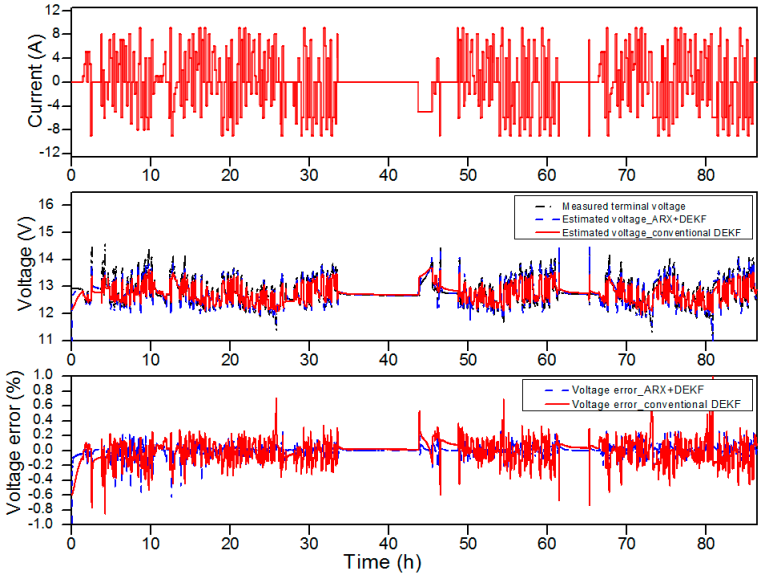

Figure 10. Comparison of the voltage estimation for the aged battery (59.3% SOH) by the proposed ARX-DEKF and conventional DEKF method.

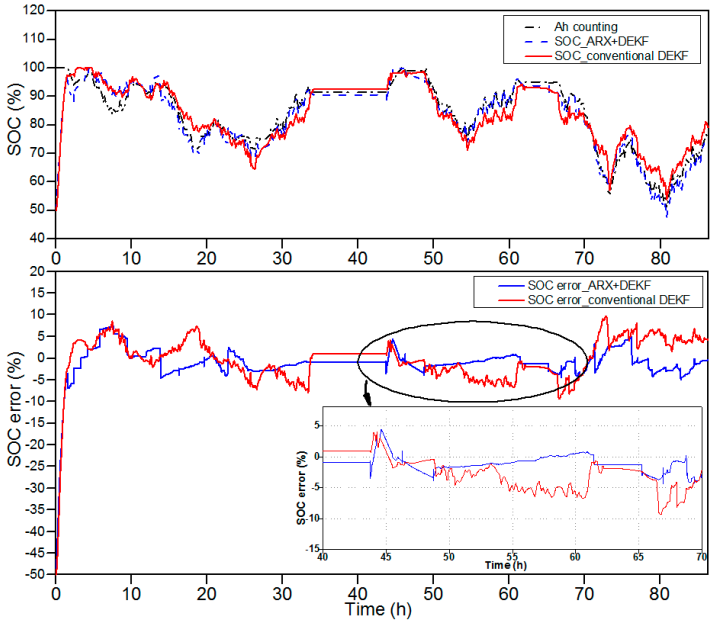

Figure 11. Comparison of the SOC estimation for the aged battery (59.3% SOH) by the proposed ARX+DEKF and conventional DEKF method.

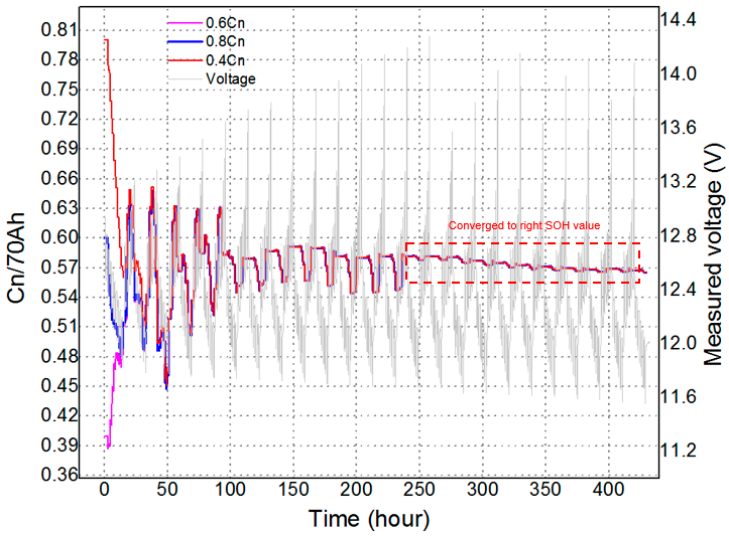

Figure 12. The convergence of the SOH estimation result with different initial capacity values (The measured capacity of the battery is 59.3% SOH).

The battery capacity estimation by the DEKF-ARX method is shown in Figure 12. Again, three different initial capacity values (0.8 Cn, 0.6 Cn and 0.4 Cn) are used in this simulation. In all three cases, the estimated values of the capacity converge to the real capacity (0.596 Cn = 41.72 Ah) within an error range of 3% in a 250 h time duration. After convergence to the correct value, the SOH has a very small change which verifies the accuracy of the proposed method. Table 1 shows that the performance of proposed method is better in terms of the root mean square errors (RMSEs) of estimated voltage and SOC when compared to the conventional method without paramter estimation.

In practical systems, the temperature can vary depending upon the external environment. To validate the proposed method under different temperatures, a random charge/discharge profile is applied to a battery having temperature variations from 25 °C to 45 °C and finally to 60 °C.

Table 1. Comparison of proposed and conventional method.

Measured Capacity (%)	RMSE of Voltage (V) by Proposed Method	RMSE of Voltage (V) by Conventional Method	RMSE SOC (%) by Proposed Method	RMSE SOC (%) by Conventional Method
98.0	0.0626	0.1015	4.5812	5.4202
75.6	0.0515	0.1234	4.4289	6.1276
60.3	0.0586	0.1252	4.2348	7.2234

RMSE means root mean square error.

At first the battery is discharged to about 50% SOC and then three cycles of 20% SOC are repeated while the temperature of the battery is manually changed at certain points as shown in Figure 13. The SOC estimation results are shown in Figure 14. These results demonstrate the accuracy of the proposed algorithm under variable temperatures. Similarly, Figures 15 and 16 represent the SOC estimation algorithm at −5 °C. The SOC of the battery is decreased from 100% to about 1% when a random current is applied to the battery. The maximum error obtained with the −5 °C profile is about 2%. This shows that whenever a continuously decreasing SOC profile is applied to a battery the estimation accuracy is better than 5% with the proposed algorithm.

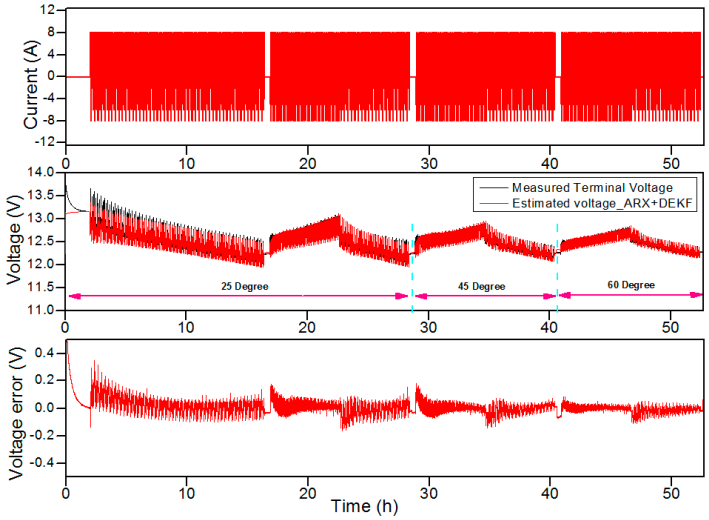

Figure 13. Current profile (upper graph), measured terminal voltage and temperature variation (middle graph) and estimated voltage error (lower graph).

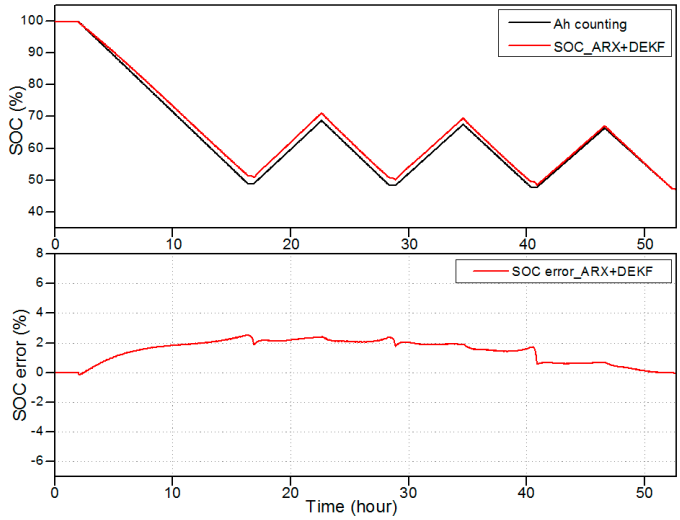

Figure 14. SOC estimation of the variable temperature profile by the proposed method.

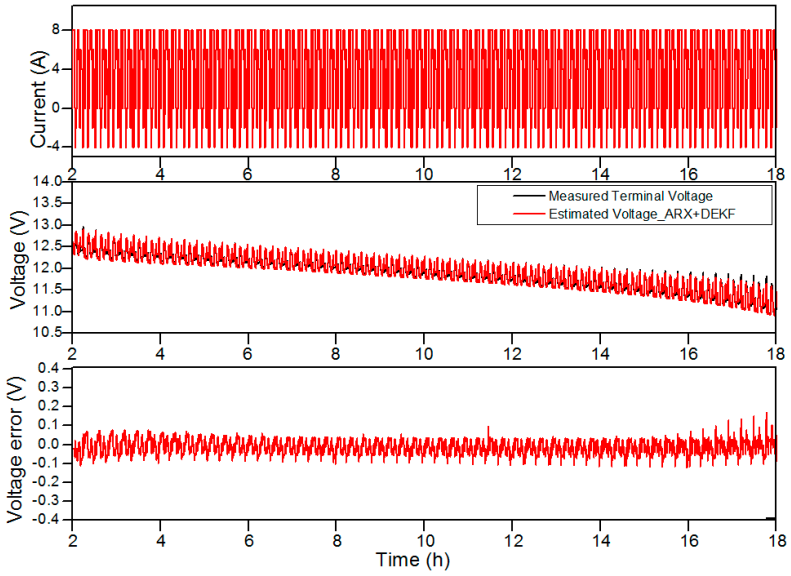

Figure 15. Current profile (upper graph), measured terminal voltage (middle graph) and estimated voltage error (lower graph) at −5 °C.

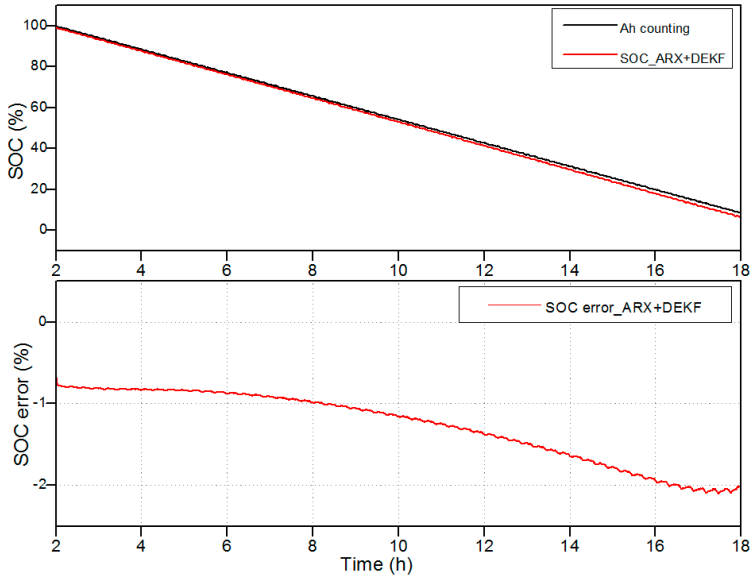

Figure 16. SOC estimation at −5 °C by the proposed method.

6. Conclusions

This paper proposed a novel method for estimating the SOC and SOH of lead-acid batteries based on a combination of online battery parameter estimation with the ARX model and the DEKF algorithm including OCV hysteresis and diffusion models. The accuracy of the battery model is validated by its ability to precisely reconstruct battery voltage during operation with a relative error of less than 0.1 V. Thus, the proposed model can accurately regenerate the voltage response of a battery under a frequent charge discharge profile. Moreover, the observed errors of the SOC estimation and SOH estimation during a random charge discharge current pulse test are within the limits of 5% and 3%, respectively. By applying the proposed method to three batteries of the same type but having different capacities, it is shown that the proposed method works successfully with aged batteries, while the conventional DEKF method gives higher estimation errors. Similarly, the proposed method is also verified under different temperatures. With the help of the proposed method, the time and labor for battery pretests

can be significantly reduced, since changes in the battery parameters are detected by the ARX and then used for updating the battery model for the DEKF. The proposed method can be used in any kind of battery management system for use in ISS systems and energy storage applications.

Acknowledgments: We want to thank the anonymous reviewers for their help in revising this manuscript.

Author Contributions: Ngoc-Tham Tran developed the basic idea behind the present research, carried out the experiments at 25 °C temperature and prepared the manuscript in the early stages. Abdul Basit Khan carried out the experiments at variable temperatures and prepared the final manuscript. Woojin Choi supervised all the main research tasks.

Conflicts of Interest: The authors declare no conflict of interest.

References

1. Le, D.; Sisk, B. Lead-Acid state of charge estimation for start-stop applications. *SAE Int. J. Altern. Power* **2013**, *2*, 172–178. [CrossRef]
2. Duong, V.H.; Tran, N.T.; Park, Y.J.; Choi, W. Novel estimation technique for the state-of-charge of the lead-acid battery by using EKF considering diffusion and hysteresis phenomenon. *Trans. Korean Inst. Power Electron.* **2014**, *19*, 139–148. [CrossRef]
3. Duong, V.H.; Tran, N.T.; Choi, W.; Kim, D.W. State estimation technique for VRLA batteries for automotive applications. *J. Power Electron.* **2016**, *16*, 238–248. [CrossRef]
4. Anbuky, A.H.; Pascoe, P.E. VRLA battery state-of-charge estimation in telecommunication power systems. *IEEE Trans. Ind. Electron.* **2000**, *47*, 565–573. [CrossRef]
5. Coleman, M.; Lee, C.K.; Zhu, C.; Hurley, W.G. State-of-charge determination from EMF voltage estimation: Using impedance, terminal voltage, and current for lead-acid and lithium-ion batteries. *IEEE Trans. Ind. Electron.* **2007**, *54*, 2550–2557. [CrossRef]
6. Coleman, M.; Hurley, W.G.; Lee, C.K. An improved battery characterization method using a two-pulse load test. *IEEE Trans. Energy Convers.* **2008**, *23*, 708–713. [CrossRef]
7. Bhangu, B.S.; Bentley, P.; Stone, D.A.; Bingham, C.M. Nonlinear observers for predicting state-of-charge and state-of-health of lead-acid batteries for hybrid-electric vehicles. *EEE Trans. Veh. Technol.* **2005**, *54*, 783–794. [CrossRef]
8. Shahriari, M.; Farrokhi, M. Online state-of-health estimation of VRLA batteries using state of charge. *IEEE Trans. Ind. Electron.* **2013**, *60*, 191–202. [CrossRef]
9. Xiong, R.; Sun, F.; Gong, X.; Gao, C. A data-driven based adaptive state of charge estimator of lithium-ion polymer battery used in electric vehicles. *Appl. Energy* **2014**, *113*, 1421–1433. [CrossRef]
10. Yuan, S.; Wu, H.; Yin, C. State of charge estimation using the extended Kalman filter for battery management systems based on the ARX battery model. *Energies* **2013**, *6*, 444–470. [CrossRef]
11. Dong, G.; Wei, J.; Zhang, C.; Chen, Z. Online state of charge estimation and open circuit voltage hysteresis modeling of $LiFePO_4$ battery using invariant imbedding method. *Appl. Energy* **2016**, *162*, 163–171. [CrossRef]
12. He, H.; Zhang, X.; Xiong, R.; Xu, Y.; Guo, H. Online model-based estimation of state-of-charge and open-circuit voltage of lithium-ion batteries in electric vehicles. *Energy* **2012**, *39*, 310–318. [CrossRef]
13. Waag, W.; Fleischer, C.; Sauer, D.U. Critical review of the methods for monitoring of lithium-ion batteries in electric and hybrid vehicles. *J. Power Sources* **2014**, *258*, 321–339. [CrossRef]
14. Xiong, R.; Gong, X.; Mi, C.C.; Sun, F. A robust state-of-charge estimator for multiple types of lithium-ion batteries using adaptive extended Kalman filter. *J. Power Sources* **2013**, *243*, 805–816. [CrossRef]
15. Plett, G.L. Extended Kalman filtering for battery management systems of LiPB-based HEV battery packs: Part 3. state and parameter estimation. *J. Power Sources* **2004**, *134*, 277–292. [CrossRef]
16. Kong-Soon, N.; Yao-Feng, H.; Chin-Sien, M.; Yao-Ching, H. An enhanced coulomb counting method for estimating state-of-charge and state-of-health of lead-acid batteries. In Proceedings of the 31st Telecommunications Energy Conference, Incheon, Korea, 18–22 October 2009; pp. 1–5.
17. Ho-Ta, L.; Tsomg-Juu, L.; Shih-Ming, C. Estimation of battery state of health using probabilistic neural network. *IEEE Trans. Ind. Inform.* **2013**, *9*, 679–685.
18. Zhang, C.; Yuhong, F.; Mi, C.C. State of charge estimation of lithium-ion batteries in electric drive vehicles using extended kalman filtering. *IEEE Trans. Veh. Technol.* **2013**, *62*, 1020–1030.

19. Chen, Q.; Jiang, J.; Liu, S.; Zhang, C. A novel sliding mode observer for state of charge estimation of EV lithium batteries. *J. Power Electron.* **2016**, *16*, 1131–1140. [CrossRef]
20. Piao, C.; Li, Z.; Lu, S.; Jin, Z.; Cho, C. Analysis of real-time estimation method based on hidden Markov models for battery system states of health. *J. Power Electron.* **2016**, *1*, 217–226. [CrossRef]
21. Kang, L.; Zhao, X.; Ma, J. A new neural network model for the state-of-charge estimation in the battery degradation process. *Appl. Energy* **2014**, *121*, 20–27. [CrossRef]
22. Weigert, T.; Tian, Q.; Lian, K. State-of-charge prediction of batteries and battery–supercapacitor hybrids using artificial neural networks. *J. Power Sources* **2011**, *196*, 4061–4066. [CrossRef]
23. Salkind, A.J.; Fennie, C.; Singh, P.; Atwater, T.; Reisner, D.E. Determination of state-of-charge and state-of-health of batteries by fuzzy logic methodology. *J. Power Sources* **1999**, *80*, 293–300. [CrossRef]
24. Shen, W.X.; Chan, C.C.; Lo, E.W.C.; Chau, K.T. Adaptive neuro-fuzzy modeling of battery residual capacity for electric vehicles. *IEEE Trans. Ind. Electron.* **2002**, *49*, 677–684. [CrossRef]
25. Ming-Fa, T.; Yi-Yuan, P.; Chung-Shi, T.; Nan-Sin, L. Modeling and estimation of state of charge for lithium-ion batteries using ANFIS architecture. In Proceedings of the IEEE International Symposium on Industrial Electronics, Hangzhou, China, 28–31 May 2012; pp. 863–868.
26. Zenati, A.; Desprez, P.; Razik, H. Estimation of the SOC and the SOH of li-ion batteries, by combining impedance measurements with the fuzzy logic inference. In Proceedings of the 36th Annual Conference of Industrial Electronic Society, Glendale, AZ, USA, 7–10 November 2010; pp. 1773–1778.
27. Lee, J.; Nam, O.; Cho, B.H. Li-ion battery SOC estimation method based on the reduced order extended kalman filtering. *J. Power Sources* **2007**, *174*, 9–15. [CrossRef]
28. Vasebi, A.; Bathaee, S.M.T.; Partovibakhsh, M. Predicting state of charge of lead-acid batteries for hybrid electric vehicles by extended Kalman filter. *Energy Convers. Manag.* **2008**, *49*, 75–82. [CrossRef]
29. Waag, W.; Kabitz, S.; Sauer, D.U. Experimental investigation of the lithium-ion battery impedance characteristic at various conditions and aging states and its influence on the application. *Appl. Energy* **2013**, *102*, 885–897. [CrossRef]
30. Shuo, T.; Munan, H.; Minggao, O. An experimental study and nonlinear modeling of discharge behavior of valve-regulated lead acid batteries. *IEEE Trans. Energy Convers.* **2009**, *24*, 452–458. [CrossRef]
31. Achaibou, N.; Haddadi, M.; Malek, A. Modeling of lead acid batteries in PV systems. *Energy Procedia* **2012**, *18*, 538–544. [CrossRef]
32. Ljung, L. *System Identification Theory for the User*; Prentice Hall PTR: Upper Saddle River, NJ, USA, 1999.